FOSSEE, IIT Bombay
OpenFOAM Research Migration Project
February 26, 2026

Modelling and Simulation of Fuel Injection during Motoring of Internal Combustion Engine

Bikash Kumar Jaiswal[1], Manjil Sitoula[2], Dhiraj Garg[3], and Pushkar Seth[4]

[1]Department of Mechanical and Aerospace Engineering, Institute of Engineering, Pulchowk Campus, Tribhuwan University

[2]Research Assistant at FOSSEE, IIT BOMBAY

[3]Assistant Professor, Department of Chemical Engineering, Shiv Nadar Institution of Eminence, NH-91, Tehsil Dadri Gautam Budhha Nagar, U.P., India-201314

[4]Engineering Technical Leader at Wabtec Corporation

Abstract

This research migration project focuses on the numerical study of non-reacting fuel spray dynamics in an internal combustion engine is presented using the open source CFD solver OpenFOAM. The investigation is conducted in three stages to meet the physical realism and to ensure the proper validation of the numerical setup.

Initially, a simple IC engine cycle simulation without fuel injection and combustion was conducted for for 6 complete cycle to validate if the setup and boundary conditions are working properly. Then fuel injection is simulated separately in a constant volume configuration to validate spray breakup, evaporation, and penetration characteristics against experimental reference setting ECN Spray A as benchmark. Subsequently, a full engine cycle comprising air intake, compression, expansion and exhaust is modeled followed by fuel injection after the compression stroke for detailed analysis of spray evolution under realistic in-cylinder conditions.

The liquid fuel is modeled by tracking individual droplets as separate particle (Lagrangian Particle Tracking Method) while the surrounding air is treated as a compressible mixture of different gases. Spray physics are modeled using established sub-models, including cone nozzle injection , Reitz-KHRT breakup, Ranz-Marshall heat transfer, and boiling evaporation. Results from the constant-volume simulations match well with the experimental measurements, especially in the early stage of the spray development. There is small over-prediction of the liquid spray length at the beginning likely due to evaporation that happens a bit slower in the model than in experiment. After the transient stage, the simulated liquid length stabilizes close to the measured quasi-steady value of 11.828 mm. Vapor penetration follows the expected momentum driven trend. The simulation captures rapid early breakup, leading to a decrease in droplet diameter from over 7 μm to around 2 μm in 0.4 ms and then stabilizes at approximately 0.5 μm. Temperature drop caused by fuel evaporation is also captured confirming proper energy exchange between phases. The work demonstrates the capability of OpenFOAM to predict evaporating spray behavior and highlights the importance of careful model calibration for accurate results.
The project aims to migrate the study by Lyle M. Picket et. al. In their work, fuel injection was simulated using the operating conditions specified by the ECN Spray A benchmark case. The numerical result obtained by them were validated against the experimental measurements published by the Engine Combustion Network (ECN). The present project follows a similar approach with the objective of implementing the methodology in OpenFOAM and applying the analysis toward realistic internal combustion engine conditions.

Migrated Paper Details

Title: Comparison of Diesel Spray Combustion in Different High-Temperature, High-Pressure Facilities Authors: Lyle M. Pickett, Caroline L. Genzale, John Manin, Lei Malbec, Luis Hermant, and others Journal/Publication: SAE International Journal of Engines (Society of Automotive Engineers, SAE [14]

Keywords: OpenFOAM, IC engine, Simulation, Adiabatic, Dynamic mesh, Engine Combustion Network (ECN)

1 Introduction

The efficiency and overall performance of Internal Combustion Engines are governed by the quality of the fuel atomization and evaporation inside the combustion chamber. Poor spray breakup and slow atomization leads to incomplete combustion, increased particulate matter (PM), unburned hydrocarbons and NO_x formation[12, 13]. The liquid fuel jet injecting from the injector nozzle undergoes a complex cascade of instabilities and breakup phenomena [15]. Primary breakup

disintegrates the continuous liquid core into ligaments and large droplets near the nozzle exit, while secondary breakup further reduces droplet size through aerodynamic forces[7]. Well-established theoretical models, such as Kelvin-Helmholtz (KH) and Rayleigh-Taylor (RT) instabilities, form the basis of widely used hybrid breakup models (eg. Reitz-KHRT model)[15]. Simultaneously, sheet-like structures formed in the near-nozzle region are often modeled using BlobSheet atomization model.

The accurate prediction of diesel spray atomization, evaporation, and mixing under engine relevant conditions remains a critical challenge in the development of high-efficiency, low emission combustion systems. To ensure a reliable validation of the numerical models, standardized experimental data measurements with well characterized boundary conditions are required. So, the Engine Combustion Network (ECN) Spray A configuration has been used as the international benchmark for diesel spray modeling [5, 12]. Spray A uses a single hole, solenoid-activated injector with n-dodecane as well as a well defined diesel surrogate, operated at a nominal rail pressure of 150 MPa, a fuel temperature of 363 K and ambient conditions of 900 K and 22.8 kg/m^3. Many experiments has been done using schlieren imaging. The fuel is injected into the cylinder under high pressure and high-temperature conditions similar to the cylinder at compressed stroke (about 60 bar and high gas density). The oxygen level in the chamber is varied from 0% for no combustion to 15 % for combustion. A large amount of detailed experimental data is freely available. This includes high-speed images from Mie-scattering and DBI techniques to measure how far the liquid fuel spray travels, as well as schlieren and extinction methods to track the speed of fuel vapor, PDPA measurements to determine droplet sizes, and Rayleigh scattering to study how well the fuel mixes with air [5]. In this study, we chose the ECN Spray A condition with 0% oxygen (non-reacting evaporating spray) as the main case to test how well the Lagrangian spray model works in OpenFOAM. We paid special attention to how the spray breaks up at the beginning and later stages, how droplet sizes change over time, and how far the liquid and vapor parts of the spray travel.

Accurate numerical representation of these competing mechanisms is essential for reliable prediction of droplet size distribution, spray penetration and fuel air mixing. The formation of air-fuel mixtures depends on various factors such as fuel characteristics, the atomization process and the evaporation characteristics. The injection pressure plays an important role in droplet break-up [10].

While constant-volume chamber studies gives excellent insight into spray physics, real diesel engine operates with a moving piston, changing volume, intake of fresh air, compression and exhaust of burned gases. To fill the gap between simplified chamber tests and actual engine conditions, this study extends the simulation of a Complete IC engine cycle including intake, compression, fuel injection, expansion and exhaust strokes both with and without fuel injection. The goal is to

understand how spray behavior changes inside a realistic moving piston environment with dynaic mesh motion and valve timing.

A diesel engine works in four main steps, called strokes. Each stroke is one movement of the piston (up or down). The full cycle takes two full turns of the crankshaft i.e. 270°.
Figure 1 shows these four strokes in a simple way.

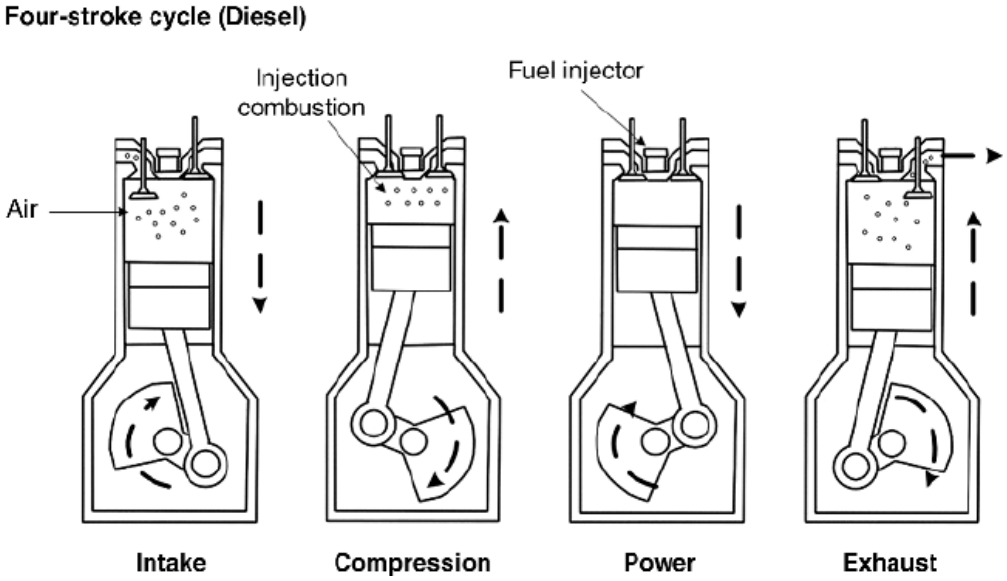

Figure 1: Working of the four stroke diesel engine cycle [8]

- **Intake**: The piston moves down from top to bottom of the cylinder. The intake valve opens and fresh air is sucked into the cylinder.
- **Compression**: The piston moves back up. Both valves are closed. The air inside gets squeezed into much smaller space. This compression makes the air very hot and increases the pressure a lot.
- **Power**: Near the top, small amount of diesel is injected directly into the hot compressed air. The fuel mixes with the air and ignites by itself because of high temperature. The burning fuel creates hot gases that expand quickly and push the piston down with great force. This is the stroke that produces power to run the engine.
- **Exhaust**: The exhaust valve opens and the burned gases are pushed put of the cylinder. The cylinder is now ready for next intake stroke.

These four strokes repeat continuously to keep the engine running.

2 Problem Statement

The primary objective of this study is to simulate the non-reacting evaporating spray characteristics and breakup of the fuel droplets of the ECN Spray A benchmark case using the open-source computational fluid dynamics (CFD) software OpenFOAM. ECN spray A provides a well-defined, extensively validated experimental dataset for high pressure diesel-like fuel injecton, enabling direct comparison between numerical prediction and measurements from multiple research institutions.

In the ECN Spray A setup, n-dodecane is injected through a single-hole nozzle straight into a still, very hot and high-pressure environment inside a fixed-volume combustion chamber.

Table 1: Nominal Operating Conditions for ECN Spray A

Parameter	**Value**
Fuel	n-dodecane ($C_{12}H_{26}$)
Injection pressure	150 MPa
Nozzle diameter	90 μm (single axial hole)
Ambient temperature	900 K
Ambient pressure	60 bar
Ambient density	22.8 kg/m^3
Ambient oxygen concentration	0%

The key quantities of interest for validation are:

Liquid penetration length: The maximum axial length of the 90% of total mass of the liquid from the injector nozzle.

Vapor Penetration: The axial distance to the farthest downstream location where the fuel mixture fraction exceeds a small threshold i.e. about 0.1% showing continuous growth with time.

Diameter distribution: The focus is on analyzing the droplet diameter distribution after breakup using the Sauter Mean Diameter (SMD) and comparing it with the Arithmetic mean diameter. This analysis provides insights into the atomization atomization quality, evaporation efficiency, and mixing behavior which are critical for predicting combustion performance in diesel-like sprays.

3 Governing Equations and Models

The spray is modeled using the Lagrangian particle tracking (LPT) approach, in which discrete droplet parcels are tracked within a continuous Eulerian gas phsase. The gas phase is treated as a compressible multi-component mixture and is described by Favre-averaged Navier-Stokes equations with additional source terms accounting for the interaction with dispersed liquid phase.

3.1 Gas-phase conservation equations

The conservation equations for the continuous phase are:

- **Mass conservation**

$$\frac{\partial \rho}{\partial t} + \nabla \cdot (\rho \mathbf{U}) = \dot{S}_m, \tag{1}$$

  where $\dot{S}_m$ is the mass source due to droplet evaporation.

- **Momentum conservation**

$$\frac{\partial (\rho \mathbf{U})}{\partial t} + \nabla \cdot (\rho \mathbf{U}\mathbf{U}) = -\nabla p + \nabla \cdot \boldsymbol{\tau} + \rho \mathbf{g} + \dot{\mathbf{S}}_p, \tag{2}$$

  where $\dot{\mathbf{S}}_p$ represents the momentum exchange with the droplets (primarily drag).

- **Energy conservation** (sensible enthalpy form)

$$\frac{\partial (\rho h_s)}{\partial t} + \nabla \cdot (\rho \mathbf{U} h_s) = \frac{\partial p}{\partial t} + \nabla \cdot (\alpha \nabla h_s) + \dot{S}_h, \tag{3}$$

  where $\dot{S}_h$ includes the energy source from convective heat transfer to droplets and the latent heat of evaporation.

- **Species conservation** (for fuel vapor Y_F)

$$\frac{\partial (\rho Y_F)}{\partial t} + \nabla \cdot (\rho \mathbf{U} Y_F) = \nabla \cdot (\rho D \nabla Y_F) + \dot{S}_m. \tag{4}$$

The system is closed with the ideal gas law $p = \rho R T$, where R is the specific gas constant for the mixture.

3.2 Adiabatic Process

In the present study, the compression and expansion processes inside the cylinder are assumed to be adiabatic, meaning that no heat transfer occurs between the working fluid and the surroundings. Under this assumption, the thermodynamic state of the gas follows the adiabatic relation derived from the first law of thermodynamics.

For an ideal gas undergoing an adiabatic process, the relationship between pressure and volume is given by

$$PV^{\gamma} = \text{constant} \tag{5}$$

where (P) is the pressure, (V) is the volume, and ($\gamma = \frac{C_p}{C_v}$) is the ratio of specific heats.

Similarly, the temperature–volume and temperature–pressure relations can be expressed as

$$TV^{\gamma-1} = \text{constant} \tag{6}$$

$$T^{\gamma}P^{1-\gamma} = \text{constant} \tag{7}$$

These relations indicate that during compression, the temperature and pressure increase as the volume decreases, while during expansion the temperature and pressure decrease as the volume increases.

In the absence of combustion, the energy variation inside the cylinder is governed primarily by the work interaction associated with piston motion and the internal energy change of the gas–fuel mixture. When fuel injection occurs, additional energy exchange takes place due to phase change (evaporation), which extracts latent heat from the surrounding gas, leading to further temperature reduction compared to the purely adiabatic case.

Therefore, the adiabatic assumption provides the baseline thermodynamic behavior of the system, while deviations from the ideal adiabatic path arise due to mass addition, evaporation, and associated energy transfer processes.

3.3 Droplet motion

The position and velocity of a droplet parcel are governed by

$$\frac{\mathrm{d}\mathbf{x}_p}{\mathrm{d}t} = \mathbf{U}_p, \tag{8}$$

$$m_p \frac{\mathrm{d}\mathbf{U}_p}{\mathrm{d}t} = \mathbf{F}_D + \mathbf{F}_g + \cdots, \tag{9}$$

where $\mathbf{F}_D = \frac{1}{8}\pi\rho_g d_p^2 C_D |\mathbf{U}_g - \mathbf{U}_p|(\mathbf{U}_g - \mathbf{U}_p)$ is the drag force with $C_D = \frac{24}{Re_p}(1 + 0.15Re_p^{0.687})$ (Schiller–Naumann correlation [16]) and $_p = \rho_g d_p |\mathbf{U}_g - \mathbf{U}_p|/\mu_g$.

3.4 Droplet temperature and evaporation

Droplet temperature evolution follows

$$m_p c_{p,l} \frac{\mathrm{d}T_p}{\mathrm{d}t} = \pi d_p \lambda_g (T_g - T_p) + \dot{m}_v L_v, \tag{10}$$

where the evaporation rate is calculated using the Spalding model [18]:

$$\dot{m}_v = \pi d_p \rho_g D_v \ln(1 + B_M), \tag{11}$$

with mass transfer number $B_M = (Y_{v,s} - Y_{v,\infty})/(1 - Y_{v,s})$.

3.5 Primary atomization - Blob-Sheet model

Near-nozzle primary breakup is modeled using the Blob-Sheet approach [17], where injected parcels are treated as spherical blobs of diameter equal to the diameter of the nozzle exit. Sheet thickness and breakup length are estimated from gas-liquid momentum balance.

3.6 Secondary breakup - Reitz-KHRT model

Secondary atomization is described by the hybrid Kelvin–Helmholtz/Rayleigh–Taylor (KH-RT) model [15, 1]:

- KH wave growth rate: $\Omega_{KH} = \frac{0.3(1+0.3Z^{0.8})\sigma}{\rho_l a^2} \left(\frac{\rho_g}{\rho_l}\right)^{0.5} {}^{0.5}$,
- Characteristic breakup time: $\tau_{KH} = 3.726 B_1 d/(\Lambda_{KH}\Omega_{KH})$,
- Child droplet diameter: $d_c = B_0 \Lambda_{KH}$,

where $= \rho_g U_{rel}^2 d/\sigma$ is the Weber number, $Z = \sqrt{}/_l$ is the Ohnesorge number, and $B_0 = 0.61$, $B_1 = 10$–40 are model constants.

Rayleigh-Taylor instabilities are included when the RT wavelength Λ_{RT} is smaller than the parent droplet diameter and the wave growth time exceeds the breakup timescale.

3.7 Sauter Mean Diameter (SMD)

The Sauter mean diameter represent the volume-to-surface-area ratio of the entire spray and can be computed as

$$d_{32} = \frac{\sum_i n_i d_i^3}{\sum_i n_i d_i^2}, \tag{12}$$

where n_i is the number of droplets in size class i. In parcel-based simulations, a mass-weighted form is often used [2]:

$$d_{32} = \frac{\sum_p m_p}{\sum_p (m_p/d_p)}, \tag{13}$$

where the sum is over parcels p. This quantity is used as the primary metric for spray atomization quality and comparison with experimental data.

3.8 Spray Models Employed

The Lagrangian spray simulation uses a comprehensive set of sub-models for injection, atomization, breakup, drag, evaporation, heat transfer, and turbulence interaction. The selected models and their key parameters are summarized in Table 2.

Table 2: Spray sub-models and parameters used in the present study

Topic	**Model and Parameters**
Turbulence closure	k-ϵ model
Injection	`coneNozzleInjection`
	Cone angle: 22° [4]
Atomization and secondary breakup	Reitz-KHRT hybrid model [4]
	$B_0 = 0.61$
	$B_1 = 18$
	$C_\tau = 1$
	$C_{RT} = 0.1$
	$C_b = B_1/2 = 9$
Collision	None (negligible influence for evaporating sprays [3])
Drag	`sphereDrag`
Evaporation	`liquidEvaporationBoil`
Heat transfer	`RanzMarshall` (with Bird correction)
Dispersion	`stochasticDispersionRAS`
Initial size distribution	Rosin-Rammler
	Sauter mean diameter $d = 6$ μm [9]
	$D_{\max} = 18$ μm
	$D_{\min} = 1$ μm
	Exponent $n = 3$ [19]

These models were chosen to accurately represent the high pressure, evaporating n-dodecane spray under ECN spray A conditions. The Reitz-KHRT breakup constants were calibrated ($B_1 = 18$) to achieve realistic droplet fragmentation and evaporation rates [3]. The Rosin-Rammler distribution with SMD of 6 μm provides a ploydisperse initial parcel population consistent with near nozzle measurements.

4 Simulation Procedure

4.1 Geometry and Mesh

The SNL GM 1.9 L Engine Geometry has taken into study for the project. This 1.9 L diesel engine has an 82 mm cylinder diameter (bore) and 90.4 mm piston travel (stroke), creating 0.477 L of

displacement per cylinder. It uses a high 15.8:1 compression ratio typical for diesel engines. The piston connects to a 166.7 mm rod with a small 1.6 mm offset. It has 23,442.5 mm^3 bowl volume which enhances air-fuel mixing and various small volumes adding up to 32.2 ml clearance space. The crankshaft's 45.2 mm radius spins at about 1500 RPM and completes one revolution in 0.04 sec. As it is a four-stroke diesel IC engine, two revolutions of crankshaft contribute to one complete cycle of the IC engine consisting of all the strokes.

The mesh is generated using the OpenFOAM utility $blockMesh$ for the base block structure. The mesh was refined near the nozzle region and along the center of the cylinder using $SnappyHexMesh$ for better prediction of the fuel breakup, vaporization and mixture of the fuel with air .

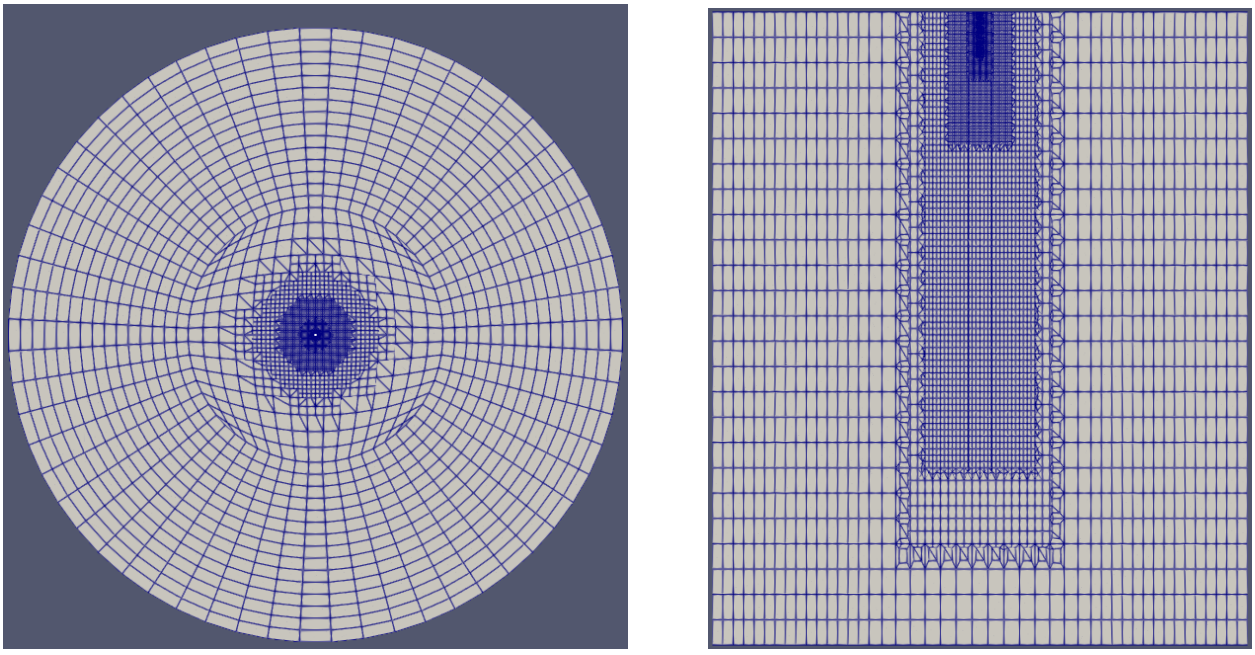

(a) Top view showing structured mesh pattern

(b) Half-section showing internal structure

Figure 2: Computational mesh used for spray simulation: (a) surface mesh topology, (b) cross-sectional view showing cell distribution and refinement near the nozzle

Table 3: Mesh Characteristics

Parameter	**Value**
Minimum Cell (along center)	0.134 mm
Maximum Cell (at the wall)	4.29 mm
Total number of cells	229,623

4.2 Mesh Independence Study

A mesh independence study was carried out for three different mesh sizes i.e. coarse, medium and fine having 117,711, 229,623 and 467,248 number of elements. The medium mesh was chosen on the basis of the values presented in Table 4.

Table 4: Mesh Independence Study

Mesh level	**Number of Elements**	**Avg. Penetration Length**	**Percentage Change**
Coarse	117,711	16.645	40.72
Medium	229,623	11.883	0.46
Fine	467,248	11.829	0.0084
Richardson Extrapolation	–	11.828	–

From the results, it is seen that the penetration length obtained using the coarse mesh is significantly different from the Richardson Extrapolation value with a percentage deviation of 40.72 %. On further refinement, the percentage change decreased to 0.46 % for the medium mesh and 0.0084 % for the fine mesh. The deviation from medium to fine mesh is less, compared to that from coarse to medium mesh, indicating monotonic grid convergence. The medium mesh is chosen since the deviation from the Richardson extrapolated value is within the desired accuracy(<1 %), and it exhibits monotonic convergence, ensuring that the solution is grid independent while avoiding the higher computational cost of the fine mesh.

4.3 Initial and Boundary Conditions

The boundary conditions applied to the velocity (**U**), pressure (p), and temperature (T) fields are summarized in Table 5. The initial conditions were prescribed as uniform throughout the computational domain.

Table 5: Boundary conditions applied to the flow variables

Boundary	**U**	p	T
Inlet	codedMixed	codedMixed	codedMixed
Outlet	codedMixed	codedMixed	zerroGradient
Top wall	noSlip	zeroGradient	zeroGradient
Cylinder wall	noSlip	zeroGradient	zeroGradient
Piston	movingWallVelocity	zeroGradient	zeroGradient

The initial conditions for all simulations were set to uniform values of pressure $p = 100$ kPa, temperature $T = 300$ K, and velocity $\mathbf{U} = (0, 0, 0)$ m/s. The boundary condition for the velocity is codedMixed such that the air intake and exhaust will take place based on the pressure and no flow occur when the valve is closed.

The initial conditions for fuel injection represent the ambient gas at rest and high pressure inside the constant-volume combustion vessel prior to the start of injection (SOI). The gas phase is initialized as uniform, with zero velocity throughout the domain. The temperature is set to the nominal experimental value of 900 K, and the pressure is uniformly initialized to approximately 60 bar to achieve the target ambient density of 22.8 kg/m^3 for the 0% O_2 case. Species mass fractions are set uniformly to replicate the non-reacting inert ambient composition, with fuel vapor mass fraction $Y_{\text{fuel}} = 0$. The gas-phase species distribution is summarized in Table 6.

Table 6: Initial ambient gas species mass fractions (non-reacting inert conditions)

Species	**Mass Fraction (Y_i)**
CO_2	0.0652
H_2O	0.0377
N_2	0.8971
O_2	0.0000
Fuel vapor	0.0000

This composition corresponds to a diluted, oxygen-free ambient typical for non-reacting evaporating spray studies, ensuring no combustion occurs while maintaining realistic thermodynamic properties and density matching the target experimental conditions. Turbulence quantities (k and ϵ) are initialized to low values consistent with a stagnant chamber ($k = 0.735$ m^2/s^2, $\epsilon = 90$ m^2/s^3).

Injection begins at $t = 0$ ms, corresponding to the actual start of injection (ASOI). Lagrangian parcels are injected using a cone injection model with a mass flow rate profile matching the experimental rate of injection for ECN spray A. The profile is typically a "top-hat" ROI that immediately reaches its steady value with a total injection duration of 1.5 ms. The profile is shown in Figure 3.

Boundary conditions are summarized in Table 7.

Table 7: Boundary conditions (ECN Spray A) during compressed state

Boundary	**Velocity (U)**	**Pressure (p)**	**Temperature (T)**
internalField	fixedValue uniform(0 0 0)	6 MPa	fixedValue 900 K
Cylinder walls	fixedValue uniform(0 0 0)	zeroGradient	zeroGradient
Top face	fixedValue uniform(0 0 0)	zeroGradient	zeroGradient
Piston	fixedValue uniform(0 0 0)	zeroGradient	zeroGradient

The internal field is initialized with zero velocity to ensure a stationary ambient gas prior to injection, a uniform pressure of 6 MPa to achieve the target ambient density of 22.8 kg/m^3 and a uniform temperature of 900 K throughout the domain. The cylinder walls, top face and piston are treated as no-slip stationary walls with zero velocity. For pressure, a zeroGradient condition

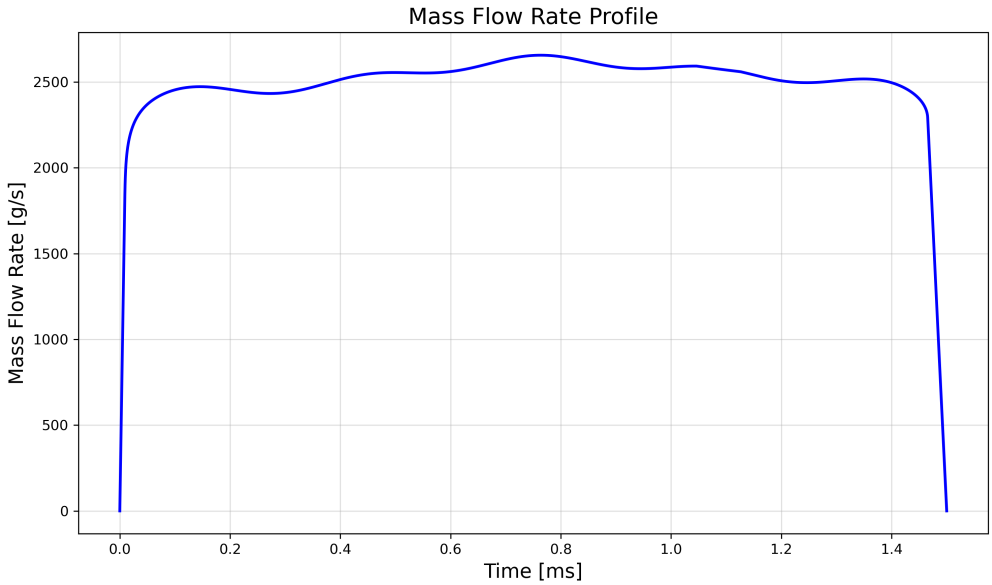

Figure 3: Mass flow rate profile used for injection (ECN Spray A nominal conditions).

is applied on all solid surface to allow normal extrapolation, consistent with impermeable walls. Temperature on the walls and piston is also set to zeroGradient assuming adiabatic conditions or negligible heat loss over short injection duration, while the top face follow the same treatment for consistency.

4.4 Solver

The simulation of the non-reacting ECN spray A case is performed using the transient, compressible, multiphase solver sprayDyMFoam. The sprayDyMFoam solver is specifically designed for dynamic mesh, unsteady evaporating sprays within a Lagrangian-Eulerian framework, making it well-suited for high pressure diesel like injection problems such as Spray A. The Eulerian gas phase solves the compressible Navier-Stokes equations for a multi-component mixture including source terms for mass, momentum, energy and species transport arising from droplet evaporation.

The numerical discretization schemes and solver settings are summarized in Tables 8 and 9.

Table 8: Discretization schemes

Scheme	**Setting**
Time derivative (ddt)	Euler (first-order implicit)
Gradient	Gauss linear
Divergence (default)	none
div(phi,U)	Gauss linearUpwind grad(U)
div(phid,p)	Gauss limitedLinear 1
div(phi,k/epsilon)	Gauss limitedLinear 1
div(phi,Yi_h)	Gauss limitedLinear 1
div(((rho*nuEff)*dev2(T(grad(U)))))	Gauss linear
Laplacian	Gauss linear orthogonal
Interpolation	linear
snGrad	orthogonal

Table 9: Solver and preconditioner settings

Variable/Group	**Solver**	**Preconditioner/Smoother**	**Tolerance / relTol**
rho / rhoFinal	PCG	DIC	1e-5 / 0.1 (0 for Final)
(U–k–epsilon) / Final	smoothSolver	symGaussSeidel	1e-6 / 0.1 (0 for Final)
p / pFinal	GAMG	GaussSeidel	0 / 0.1 (1e-6 / 0 for Final)
(Yi–O2–N2–H2O) / h	PBiCGStab	DILU	1e-6 / 0 (0.1 for h)

4.5 Piston Movement

The computational modeling of the piston-cylinder assembly employed a cylindrical domain to accurately represent the physical geometry. Using OpenFOAM's blockMesh utility, the domain was discretized with a structured hexahedral mesh featuring uniform grading (simpleGrading (1 1 1)) across all sub-regions to ensure consistent mesh quality. To capture the piston's reciprocating motion, a dynamic meshing approach was implemented, incorporating topological changes and cell deformation algorithms. Initial simulations began with the domain at top dead center (TDC), with the mesh progressively compressing toward bottom dead center (BDC). However, this configuration led to severe mesh distortion and numerical instabilities prior to reaching full compression. After careful analysis, the reference configuration was inverted - initiating the simulation at BDC and expanding outward. This revised approach significantly improved mesh preservation throughout the stroke, maintaining better cell quality metrics during deformation. The solution demonstrated robust convergence characteristics while accurately replicating the piston's kinematic motion, as verified against theoretical displacement curves. The successful implementation of this dynamic meshing strategy enabled precise tracking of fluid domain changes during the complete compression-expansion cycle.

The displacement of the piston in the cylinder can be derived as,

$$x(\theta) = r + l - \left(r\cos\theta - \sqrt{l^2 - (r\sin\theta + e)^2} \right) \tag{14}$$

where $x(\theta)$ is the piston displacement,
r is the crank radius,
l is the length of the connecting rod,
e is the perpendicular offset distance between the cylinder axis and the crankshaft center, and
θ is the crankshaft rotation angle.

The piston movement vs time is shown in Fig:4

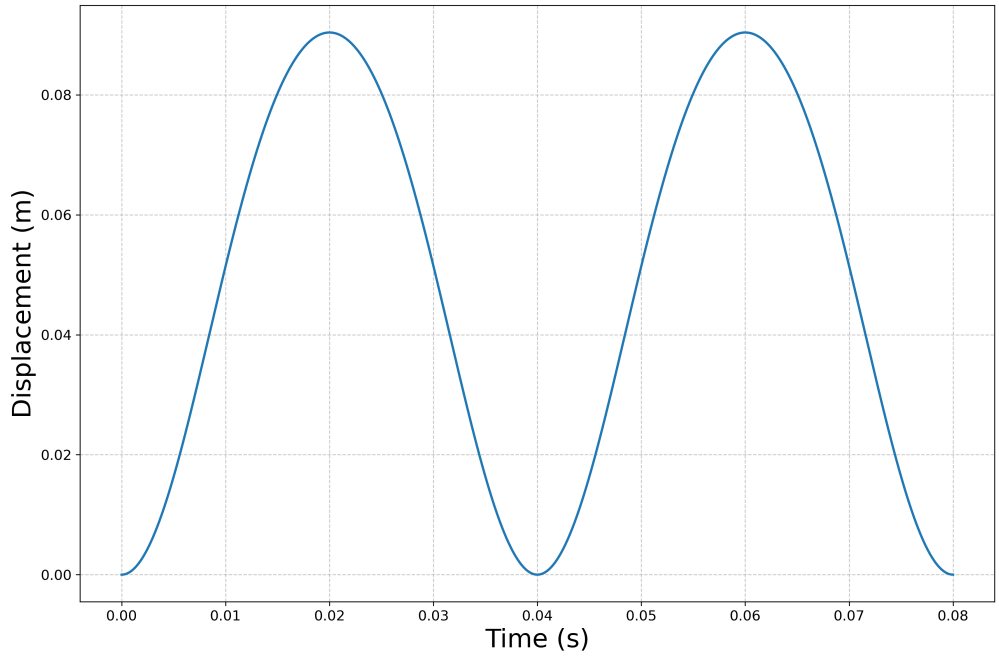

Figure 4: Displacement of piston vs time for a single cycle.

5 Results and Discussion

Initially, the numerical framework was validated by simulating six complete engine cycle encompassing intake, compression, expansion and exhaust processes to ensure stable and physically consistent piston and valve operation. Following this, the fuel injecion model was independently validated under constant volume conditions using ECN Spray A experimental benchmark, allowing assessment of spray breakup, fuel evaporation and penetration characteristics without the influence of in-cylinder flow dynamics. After successful validation of both the engine cycle dynamics and the

injection model, a fully coupled simulation incorporating air intake, compression, fuel injection, expansion and exhaust was performed to analyze the complete engine operating cycle.

5.1 Validation of Numerical Framework

The simulation was run without fuel injection initially to study only the intake, compression, expansion and exhaust of air. This helps validate the piston motion, valve timing, and boundary conditions are working correctly before adding fuel and combustion. A key diagnostic for assessing the setup is the total gas mass, average temperature, pressure and density inside the cylinder.
Figure 5a presents the variation of total mass in the cylinder with time over six cycles. The periodic rise and fall in mass confirm proper operation of the time-dependent pressure boundary conditions that simulate valve opening and closing. The timing of valve events in each cycle is summarized in Table 10.

Table 10: Valve timing in each engine cycle

Time interval (s)	**Valve state**
0–0.02	Inlet valve open (intake phase)
0.02–0.04	All valves closed (compression phase)
0.04–0.06	All valves closed (expansion phase)
0.06–0.08	Exhaust valve open (exhaust phase)

The observed mass behavior aligns well with the prescribed valve schedule: mass increases during the intake period (0–0.02 s) due to inflow through the inlet, remains nearly constant when both valves are closed, and decreases during the exhaust period (0.06–0.08 s) as gas is expelled through the outlet.
The pressure-time plot in Fig: 5cshows peak during each cycle corresponding to the compression stroke as the piston approaches top dead center (TDC). The pressure rises rapidly due to volumetric compression of the trapped air, reaching maximum values of approximately 4-5 MPa. Following the compression phase, the pressure decreases sharply during the expansion stroke as the piston moves downward. During the intake and exhaust strokes, the pressure remains comparatively low, approaching near-ambient levels.
The density variation as shown in Fig:5b closely follows the pressure evolution, consistent with the ideal gas behavior under compression and expansion. As the cylinder volume decreases during compression, the air density increases substantially, attaining its maximum near TDC. Conversely, density decreases during the expansion, intake and exhaust processes due to increasing cylinder volume and the introduction of fresh air. This trend confirms the correct representation of volumetric effects withing the computational model.

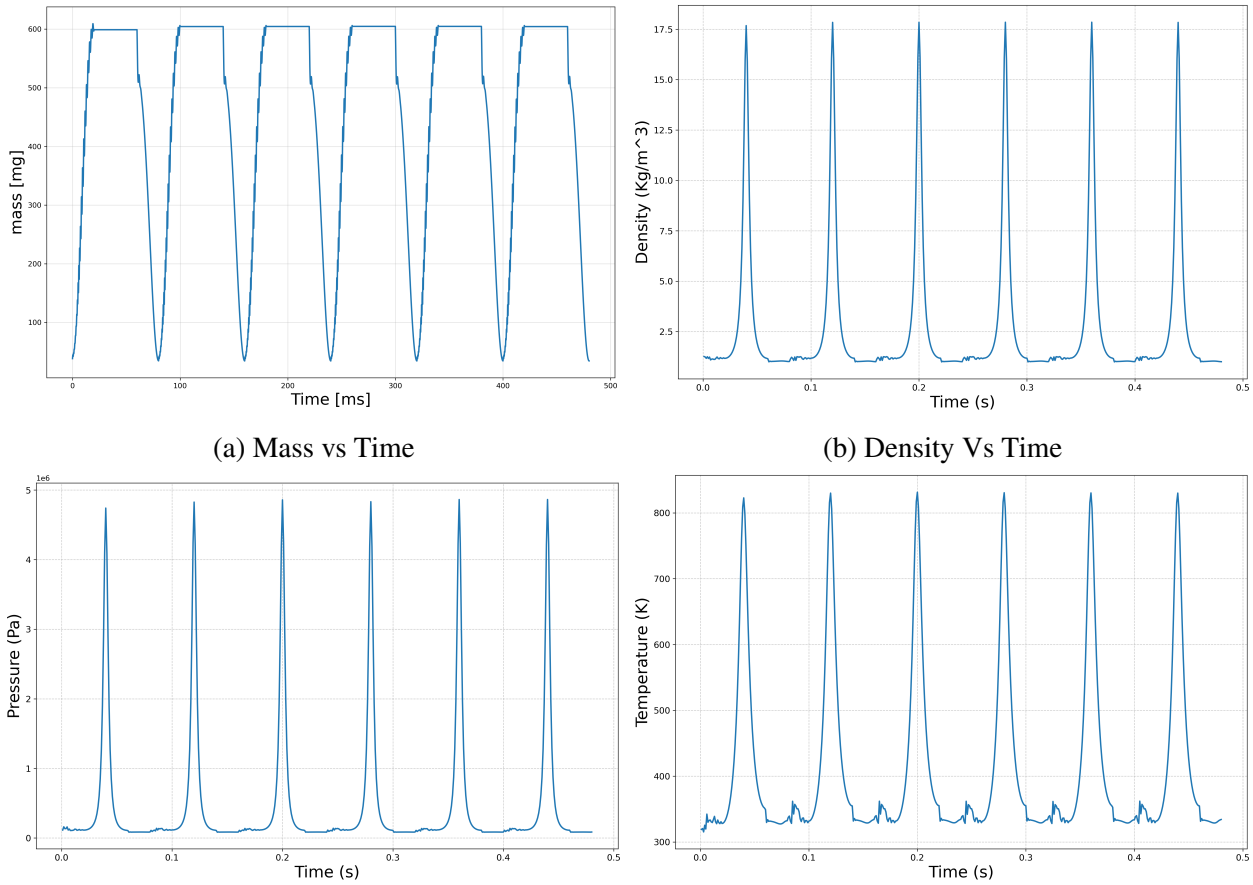

(a) Mass vs Time

(b) Density Vs Time

(c) Pressure Vs Time

(d) Temperature Vs Time

Figure 5

The temperature-time profile shown in Fig:5d demonstrate a significant rise during the compression stroke, driven by adiabatic heating of the air. Peak temperatures in the order of 900-950 K are observed near TDC, despite the absence of combustion. Subsequently, the temperature decreases during the expansion stroke due to decrease in pressure and further reduces during intake process as cooler air enters the cylinder.

Across all six cycles, the pressure, density and temperature traces exhibit high repeatability, indicating stable periodic operation. The consistent cycle-to-cycle behavior suggests that the piston motion, valve boundary conditions and the numerical setup are correctly implemented. Overall, the results demonstrate physically realistic in-cylinder thermodynamic behavior for an IC engine simulation.

5.2 Fuel Injection Model

A qualitative visualization of the simulated spray plume is presented in Figure 6, showing an iso-contour of the liquid volume fraction at a representative time.

Figure 6: Simulated spray plume structure for the non-reacting ECN Spray A case.

The contour reveals a narrow, penetrating liquid core near the nozzle transitioning to a broader evaporating plume downstream consistent with the high momentum diesel-like injection under evaporating conditions. The elongated, conical shape with dense liquid near the axis matches typical experimental visualizations of ECN Spray A obtained via high-speed shadowgraph or schlieren imaging [13].

5.2.1 Liquid Penetration

The experimental data exhibit a rapid initial rise in liquid length, reaching a quasi-steady value of approximately 10.1-10.2 mm between 0.2 and 1.5 ms ASI. This behavior is characteristic of evaporating sprays under ECN Spray A conditions, where the liquid length is controlled by the balance between injection momentum and evaporation rate.

The simulation initially over predicts the liquid penetration, reaching approximately 22 mm at 0.4 ms ASI. The excessive early penetration indicates insufficient evaporation during the transient phase likely due to delayed secondary breakup and larger initial droplet sizes, resulting in reduced surface area for heat transfer and vaporization.

However, after 0.4 ms, the simulated penetration stabilizes and oscillates around 13-14 mm. The good agreement in the quasi-steady state validates the overall modeling approach including the calibrated Reitz-KHRT breakup constants, Ranz-Marshall heat transfer and liquidEvaporationBoil model. Overall, the simulation successfully reproduces the evaporation-limited quasi-steady liquid length characteristic of ECN Spray A, with minor discrepancies confined to the early injection phase.

5.2.2 Vapor Penetration Length

Vapor penetration length is defined as the axial distance to the farthest point where the fuel mixture fraction exceeds a threshold value of 0.001, consistent with ECN Spray A standards [5].

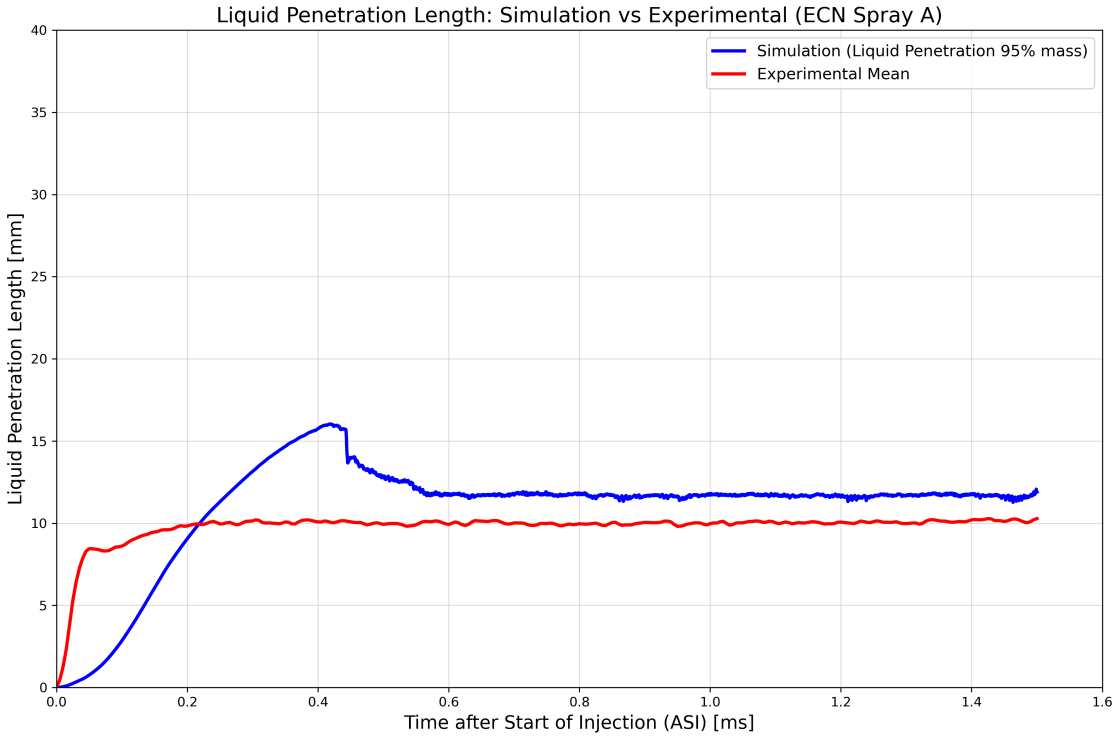

Figure 7: Liquid penetration length as a function of time after start of injection (ASI). Simulation results (blue) are compared with experimental mean (red) [6].

Figure 8 compares the simulated vapor penetration length with the experimental mean from the ECN Spray A dataset.

The experimental data exhibit a rapid initial increase, following an approximately linear trend before reaching approximately 55 mm by 1.4 ms ASI. This behavior reflects the momentum-dominated plume expansion and mixing with surrounding still air.

The simulation, using the Reitz-KHRT breakup model with calibrated constants ($B_1 = 18$), captures the qualitative trend of continuous vapor growth but under-predicts the penetration rate initially at 0-0.4 ms, which is due to poor vaporization and insufficient breakup of the fuel, as was also observed in liquid penetration However, after 0.4 ms, it starts to approach the experimental measurements showing good agreement with it.

This discrepancy is primarily attributed to reduced momentum transfer from the liquid phase, potentially due to the breakup model producing slightly larger droplets than optimal (as indicated by the SMD values in fig 10), which delays evaporation and vapor production. Additionally, the RANS turbulence modeling (standard k-ε) may under-estimate injection rates compared to LES approaches commonly used in validated ECN simulations [19].

Overall, the vapor penetration results provide good qualitative validation of the spray modeling framework, with opportunities for refinement to achieve closer quantitative alignment with the ECN

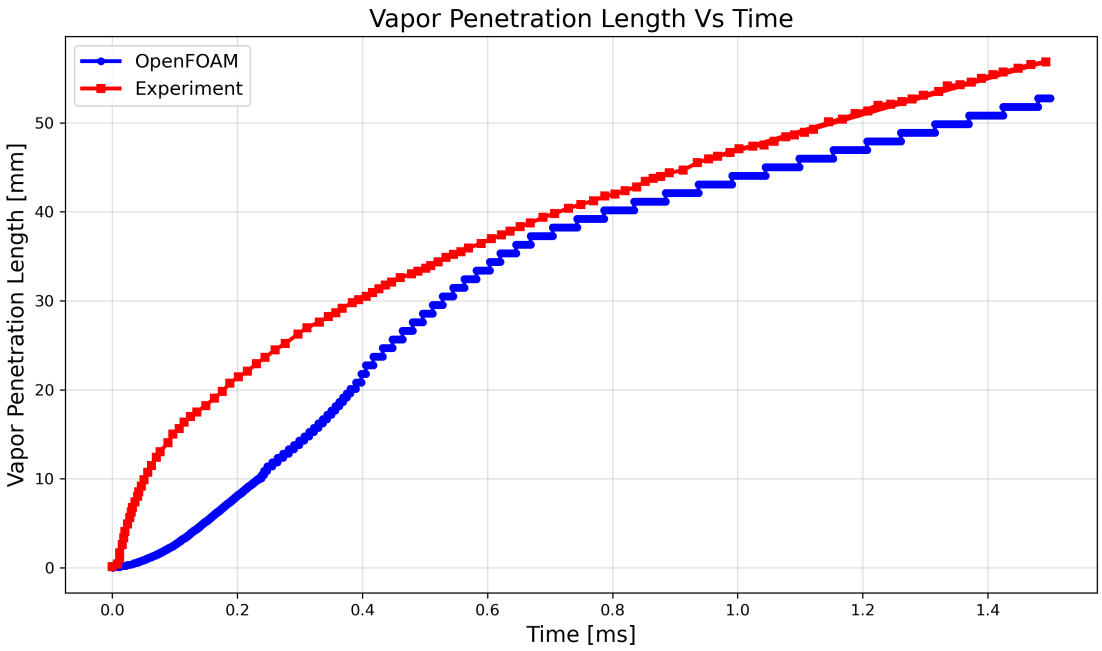

Figure 8: Vapor penetration length vs. time after start of injection (ASI) for the non-reacting ECN Spray A case. OpenFOAM simulation results (blue) are overlaid with the experimental mean (red) [6]

benchmark.

5.3 Injected and Evaporated Mass Comparison

Fig:9 shows the cumulative fuel mass injected into the domain and the cumulative mass transfer due to phase change during the spray simulation. The injection process starts at the beginning of the simulation and exhibits a smooth, monotonic increase in injected mass with time indicating a stable and well-resolved fuel delivery through the injector.

The cumulative injected mass reaches a final value of 3.56 mg which is equal to the total mass injected showing the mass flow rate shown in fig:3. The absence of oscillations in the injection curve confirms that the injection model and time integration are numerically stable.

The cumulative mass transfer due to phase change follows a similar trend but with a slight delay relative to the injected mass. This delay represents the physical time required for droplets to heat up and undergo evaporation after entering the computational domain. As the spray develops, the evaporation rate increases and the phase change curve gradually approaches the injected mass curve. By the end of the simulation, the total evaporated mass reaches to 3.56 mg showing an evaporation efficiency of 100%.

Overall, the agreement between the injected and evaporated mass curves at later times demonstrates

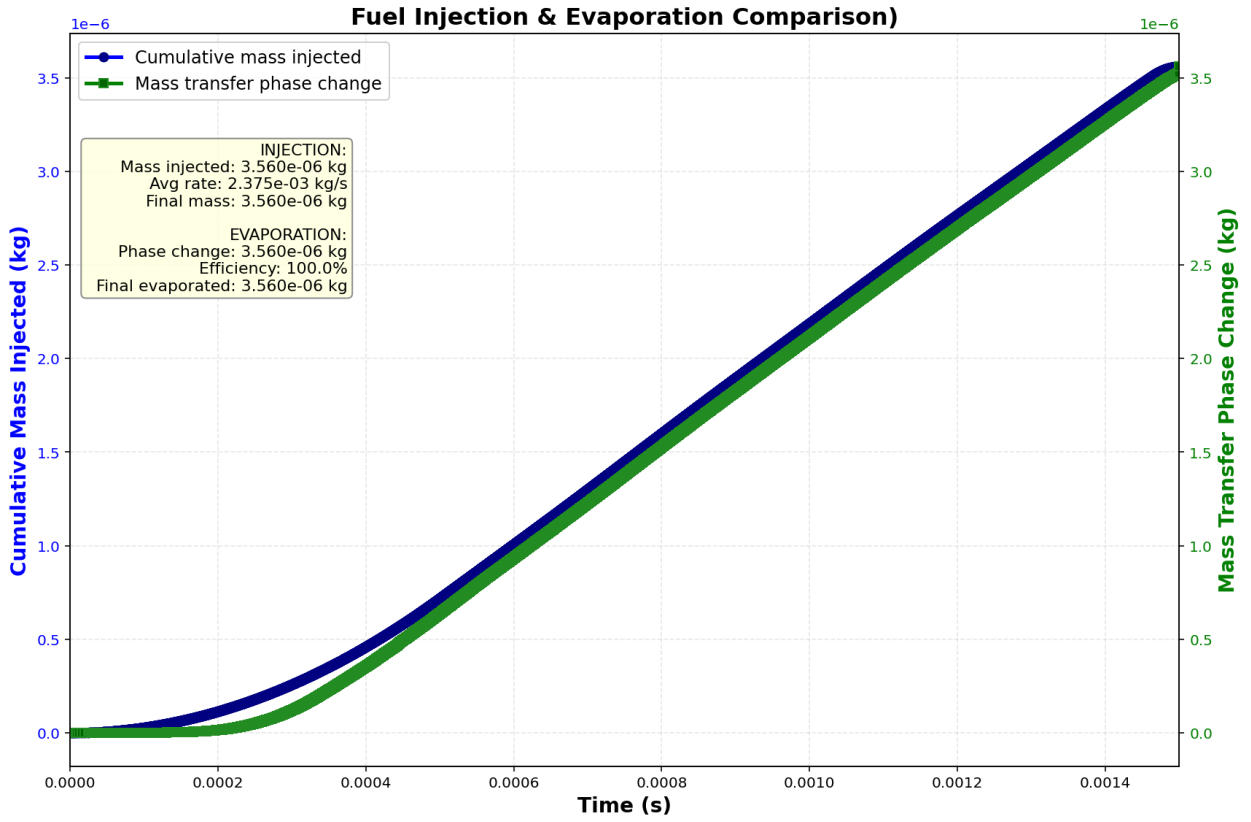

Figure 9: Comparison of mass of fuel injected and the fuel evaporation

consistent coupling between the spray injection, heat transfer and phase-change sub-models and confirms the physical credibility of the spray evaporation process in the present simulation.

5.3.1 Droplet Size Distribution

The atomization quality of the spray is evaluated through the evolution of characteristic droplet diameters, as shown in Figure 10. The plot presents values of the maximum droplet diameter ($D_{\max}$), Sauter Mean Diameter (SMD, D_{32}), and Arithmetic Mean Diameter (AMD, D_{10}) computed using the Reitz-KHRT secondary breakup model [15, 1].

The maximum droplet diameter ($D_{\max}$) initiates near the nozzle diameter (90 μm) and exhibits a rapid increase in the early injection phase (0-0.08 ms), peaking at approximately 17 μm before gradually decreasing to 8 μm by 0.5 ms. This trend reflects the initial dominance of primary injected parcels followed by progressive fragmentation driven by aerodynamic (KH) and accelerative (RT) instabilities.

The Sauter Mean Diameter (SMD) starts at lower values (7 μm) and rises to a quasi-steady level of 1-2 μm after 0.4 ms, remaining relatively constant during the main injection period. The Arithmetic Mean Diameter (AMD) stabilizes earlier at approximately 1 μm, highlighting the

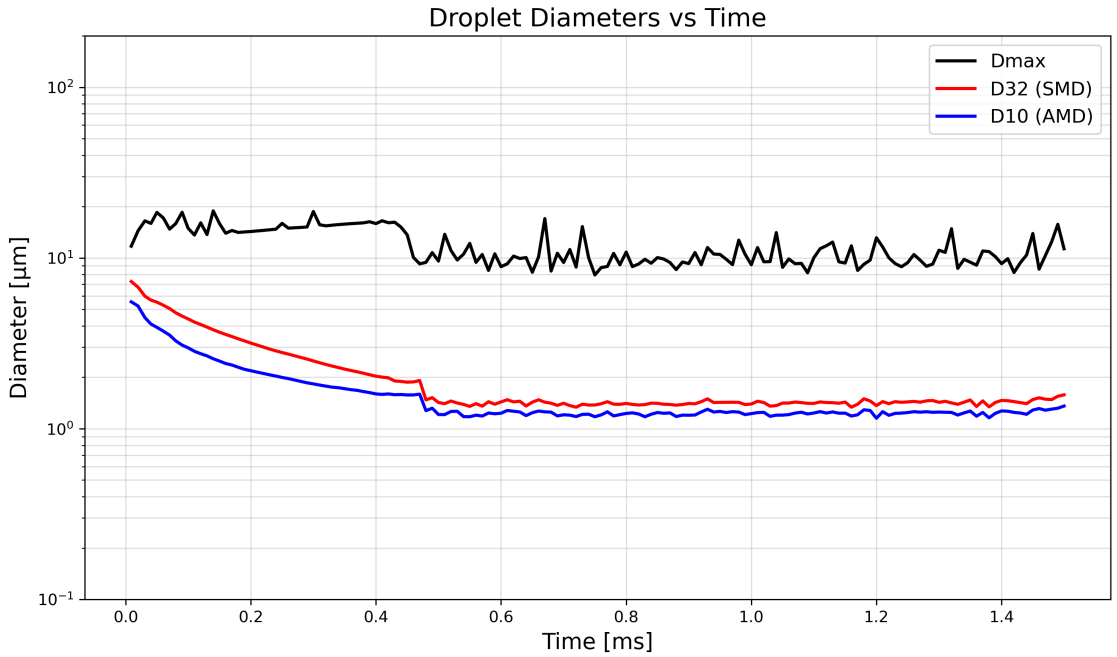

Figure 10: Temporal evolution of droplet diameters ($D_{\max}$, D_{32} (SMD), and D_{10} (AMD)) in the simulated spray under Reitz-KHRT breakup modeling.

production of numerous smaller droplets via secondary breakup.

The ratio $D_{32}/D_{10} \approx 1.2$–$1.5$ in the quasi-steady regime indicates indicates a narrow, nearly monodisperse droplet size distribution.measurements [13, 11].

The qualitative trends—rapid initial reduction in mean diameters followed by stabilization—are well captured, confirming effective activation of the Reitz-KHRT model. Quantitative improvement through constant tuning is recommended to better reproduce experimental atomization characteristics and support accurate prediction of liquid penetration and evaporation.

5.3.2 Mixture Fraction in the Chamber

Figure 11 presents the variation of the spatially averaged mixture fraction in the combustion chamber during the injection event.

The mixture fraction is initially zero throughout the domain, reflecting the pure oxidizer (air) ambient condition before fuel injection. Following the start of injection, the mixture fraction rises rapidly during the early phase as liquid n-dodecane droplets evaporate and mix with the surrounding gas. The value stabilizes around 0.01 after approximately 0.6 ms and remains nearly constant thereafter, with only minor fluctuations.

This behavior is expected in a non-reacting evaporating spray simulation. The initial sharp increase corresponds to the rapid vaporization of fuel droplets near the injector, releasing fuel

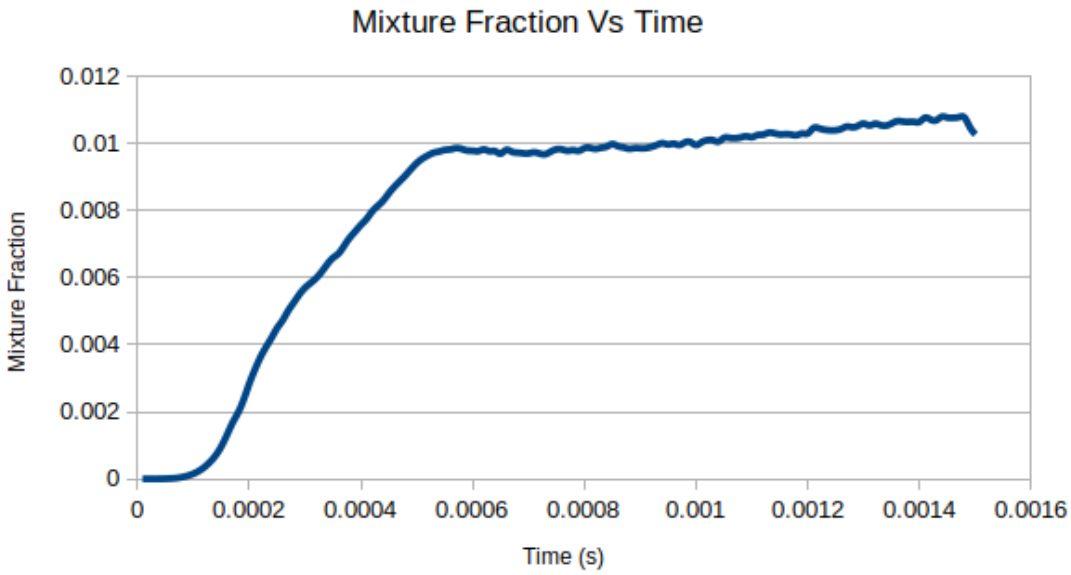

Figure 11: Spatially averaged mixture fraction in the chamber as a function of time after start of injection (ASI).

vapor into the gas phase. Once the majority of the injected fuel has evaporated, the mixture fraction approaches an equilibrium value determined by the total injected fuel mass relative to the chamber gas mass. The small magnitude (≈ 0.01) indicates a globally lean mixture, consistent with the low fuel loading typical for the ECN Spray A non-reacting case.

The near-constant mixture fraction after the initial rise confirms stable mixing and the absence of significant further evaporation or transport effects in the later stages. This result validates the correct implementation of the fuel species transport and evaporation models, showing that the simulation accurately captures the fuel-air mixing process driven by spray evaporation and turbulence.

5.3.3 Temperature Evolution in the Chamber

Figure 12 shows the temporal variation of the spatially averaged gas temperature in the chamber during the injection event.

The initial temperature is uniform at 900 K, matching the preheated ambient condition specified for the non-reacting ECN Spray A case. Shortly after the start of injection, the temperature begins to decrease, dropping by approximately 30-32 K over the 1.5 ms injection duration.

This gradual cooling is primarily attributed to the endothermic nature of fuel evaporation. As n-dodecane droplets absorb latent heat from the surrounding hot gas to vaporize, energy is extracted from the gas phase, resulting in a measurable reduction in bulk temperature. The oscillatory

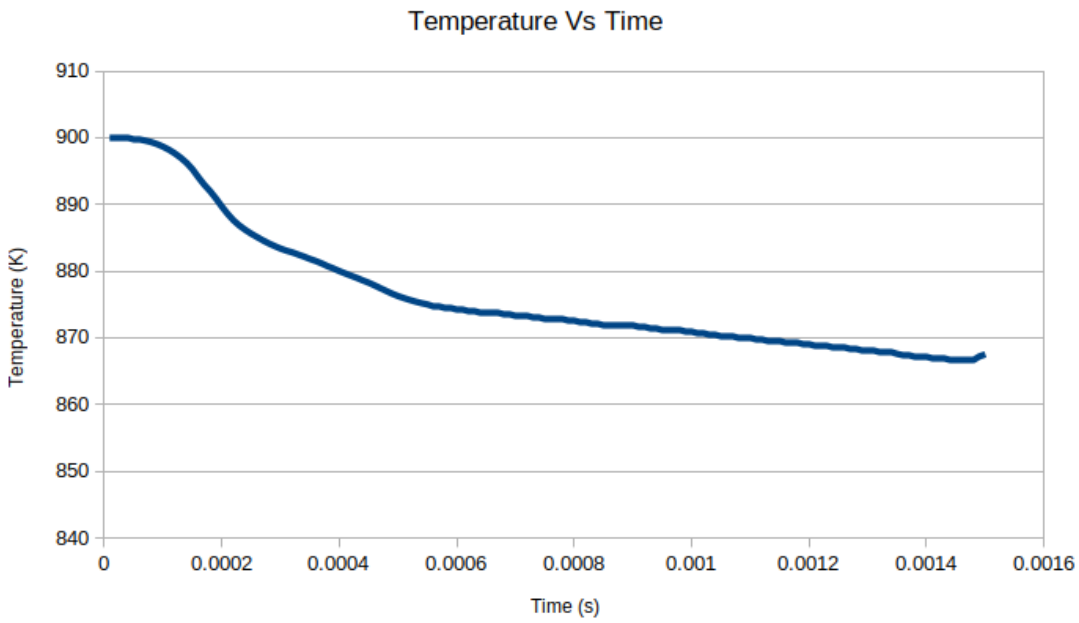

Figure 12: Spatially averaged gas temperature in the chamber as a function of time after start of injection (ASI).

behavior observed in the temperature trace is characteristic of the transient heat transfer and evaporation processes, particularly during the early stages when droplet heating and vaporization rates are highest.

The magnitude of the temperature drop is consistent with expectations for an evaporating spray where evaporation is the dominant cooling mechanism in the absence of combustion. The relatively small overall decrease ($\approx 3.5\%$) confirms that the injected fuel mass is modest compared to the chamber gas mass, preventing excessive cooling that could alter the thermodynamic state significantly.

This result validates the correct implementation of the coupled heat transfer and evaporation models (Ranz–Marshall correlation with Spalding mass transfer), demonstrating the simulation's ability to capture the energy exchange between the liquid and gas phases accurately.

5.3.4 Pressure Evolution in the Chamber

Figure 13 shows the temporal variation of the spatially averaged gas pressure in the chamber during the injection event.

The initial pressure is uniform at 60 bar (6 MPa), corresponding to the compressed ambient condition typical for the non-reacting ECN Spray A benchmark. Following the start of injection, the pressure gradually decreases, dropping by approximately 30 KPa over the 1.5 ms injection

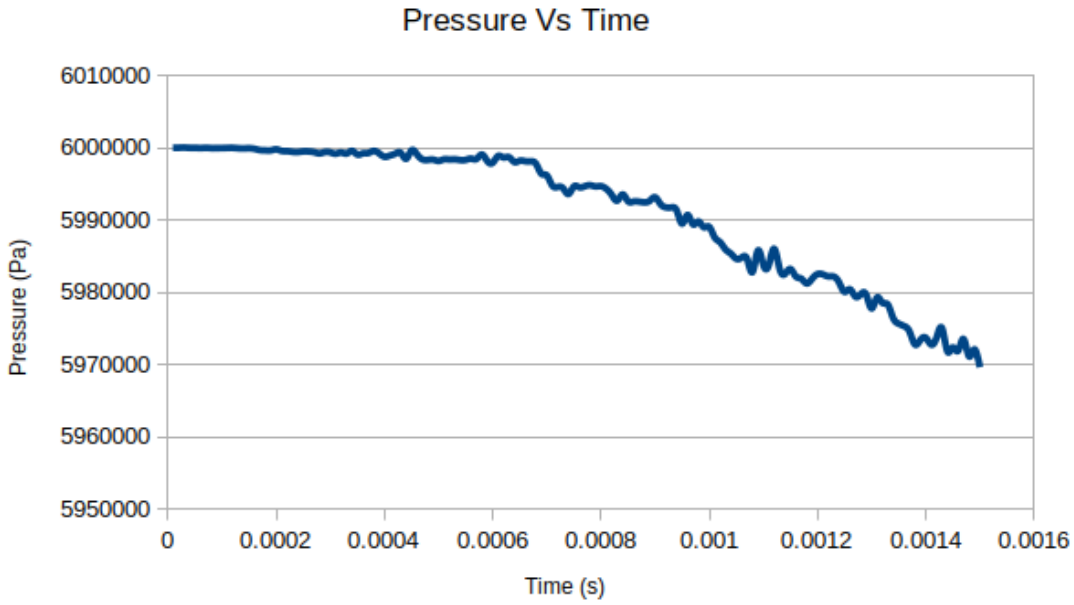

Figure 13: Spatially averaged gas pressure in the chamber as a function of time after start of injection (ASI).

duration. This pressure reduction is mainly caused by the evaporative cooling effect: as fuel droplets vaporize, they absorb thermal energy from the gas phase, leading to a slight decrease in gas temperature and, consequently, pressure (via the ideal gas law).

The smooth and continuous decline in pressure, with minor oscillations, reflects the transient nature of droplet heating, evaporation, and mixing processes. The overall pressure drop remains small (5%), which is expected given the limited fuel mass injected relative to the large gas volume in the chamber. This behavior confirms that the evaporation process does not drastically alter the chamber's thermodynamic state, maintaining conditions close to the initial high-pressure environment.

This pressure trend further validates the implementation of the phase-change model and the coupling between mass, momentum and energy transfer in the simulation. It also highlights the role of fuel evaporation as a key mechanism influencing the gas-phase pressure during the injection period in non-reacting conditions.

Overall, the initial results demonstrate correct implementation of the spray modeling framework in OpenFOAM, with realistic early-stage penetration behavior. Extension of the computational time is the primary requirement to enable meaningful quantitative comparison with the ECN Spray A benchmark data.

5.4 Overall motoring condition of IC engine along with fuel injection

This simulation include the complete IC engine cycle for motoring condition. Initially, the air is sucked inside the cylinder during the suction stroke through the inlet valve and after the suction stroke, the inlet valve closes and the air is compressed. After compression, fuel ($C_{12}H_{16}$) is injected through the fuel injector for 1.5 ms but no combustion will occur. For the current study combustion is not included. Then the air is expanded. Then the exhaust valve open and all the air is expelled through the outlet valve.

5.4.1 Mass, Pressure, Temperature and Density Variations

Figure 14a shows how the total mass inside the cylinder changes over six complete engine cycles. At the start of the cycle, the total mass inside the cylinder goes up during the intake stroke because fresh air flows in through the open inlet valve. After the intake valve closes, the mass stays almost the same during the compression stroke. Then, right after compression, the mass increases a little bit because fuel is injected into the cylinder. This causes a small but sudden increase in mass and the extra mass is exactly equal to the amount of fuel that was sprayed in. After fuel injection, the mass remains constant during the rest of the cycle until the exhaust stroke begins. As the exhaust valve opens and the mass decreases as the gases are pushed out of the cylinder through the outlet. The fact that the mass returns to the starting value at the end of the cycle proves that mass is conserved in the simulation.

Fig:14b illustrates the pressure variation over the cycle. The pressure rises sharply during the adiabatic compression phase and then falls again during the adiabatic expansion phase. The drop in pressure during expansion is partly caused by the energy absorbed when the fuel evaporates, as shown in fig:13.

Similarly, the density variation as shown in Fig:14c closely follows the pressure evolution, consistent with the ideal gas behavior under compression and expansion. As the cylinder volume decreases during compression, the air density increases substantially, attaining its maximum near TDC. Conversely, density decreases during the expansion, intake and exhaust processes due to increasing cylinder volume and the introduction of fresh air. This trend confirms the correct representation of volumetric effects within the computational model.

Similarly, Fig: 14d illustrates temperature variation over the cycle for 6 cycles. The suction takes place at constant temperature and the temperature increases during adiabatic compression and subsequently decreases during the adiabatic expansion phase. But there is sudden increase in temperature at the exhaust stroke which is not expected. The temperature at the exhaust stroke should be less than that of the suction phase since heat is extracted by the fuel for evaporation as

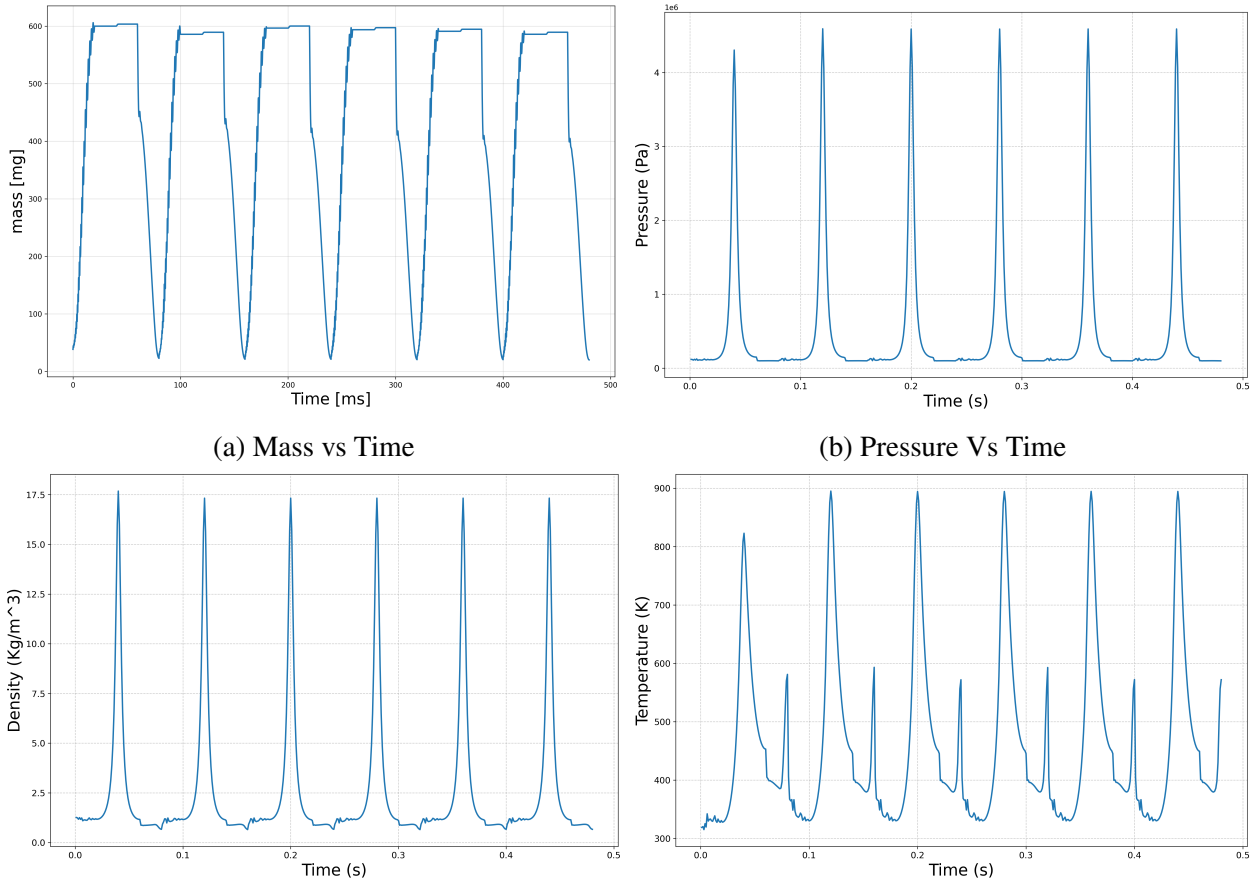

(a) Mass vs Time

(b) Pressure Vs Time

(c) Density Vs Time

(d) Temperature Vs Time

Figure 14

illustrated in fig: 12.

5.4.2 Liquid and Vapor Penetration Length

Figure 15 shows fuel penetration length during fuel injection period for complete IC engine cycle. Fuel was injected starting at 40 ms after the start of the cycle and lasted for 1.5 ms.
The penetration length start at nearly zero when leaves the injector and then travel in the cylinder upto 15 mm at ≈ 40.8 ms and then penetration slightly decreases and stabilizes around 14 mm due to vaporization of the fuel.

This behavior is expected in a non-reacting diesel spray under high-pressure and temperature condition (compressed state). The fast initial penetration is driven by the high injection momentum and the later stabilization occurs as the spray breaks up and evaporates reducing the amount of

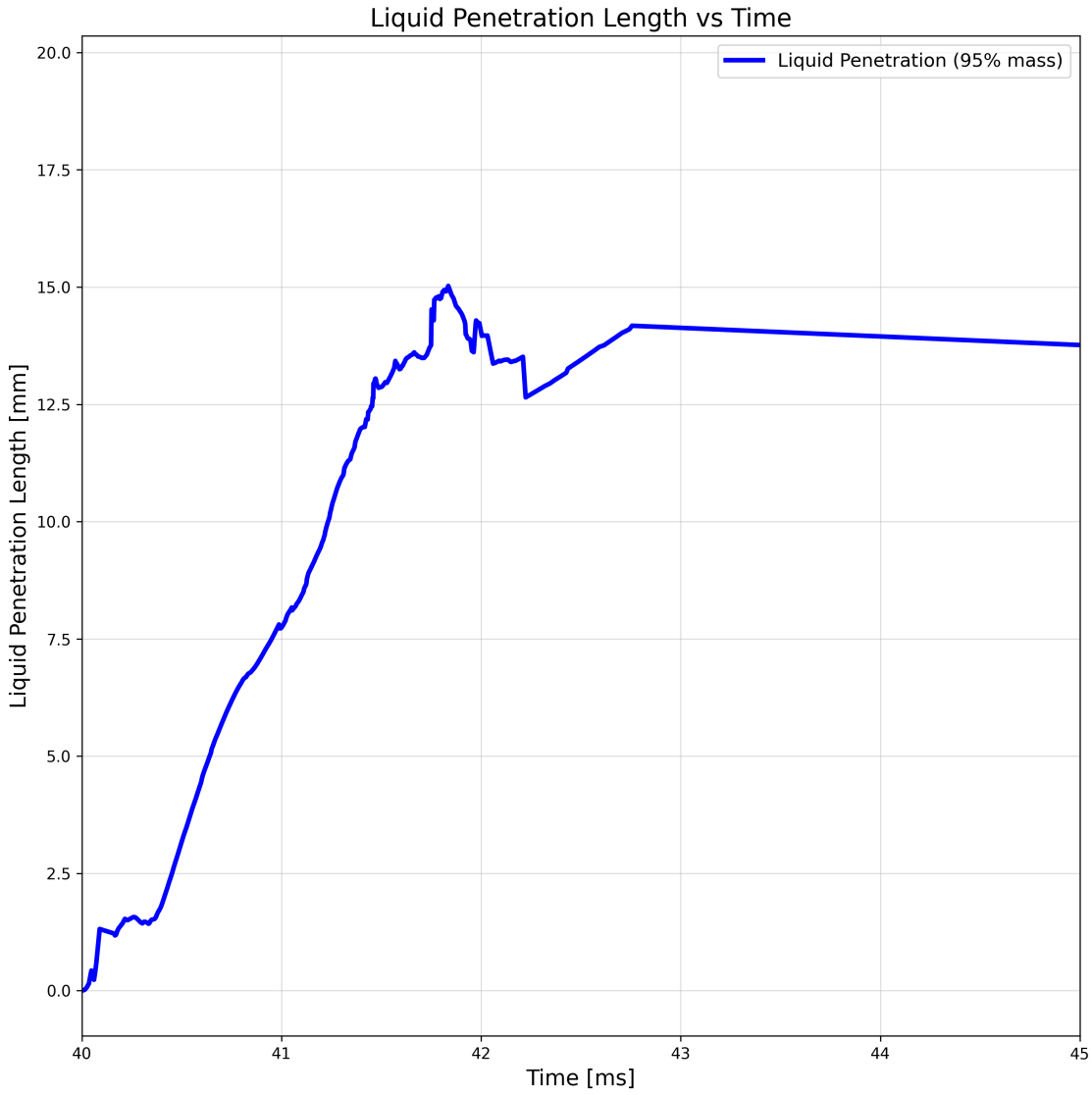

Figure 15: Fuel penetration length inside the cylinder after the start of injection at 40 ms in the compressed state

liquid inside the cylinder. The small oscillations after the peak are due to the droplet breakup and mixing with the surrounding air. Overall, penetration curve matches typical ECN spray A behavior confirming that the spray models are working correctly even inside the moving piston engine environment.

Similarly, fig 16 shows the vaporized fuel penetration length inside the cylinder. Initially, the vapor penetration length matches the behavior of the vapor penetration seen in the experimental data provided by ECN Spray A and then the vapor reaches the bottom of the piston and then move along with the piston and the vapor penetration length reaches to 96.86 mm which is the length of the cylinder. Since there is absence of combustion, the fuel vapor remains in the cylinder until exhaust.

Overall, the vapor penetration curve matches typical ECN spray A until it reaches the bottom of the cylinder.

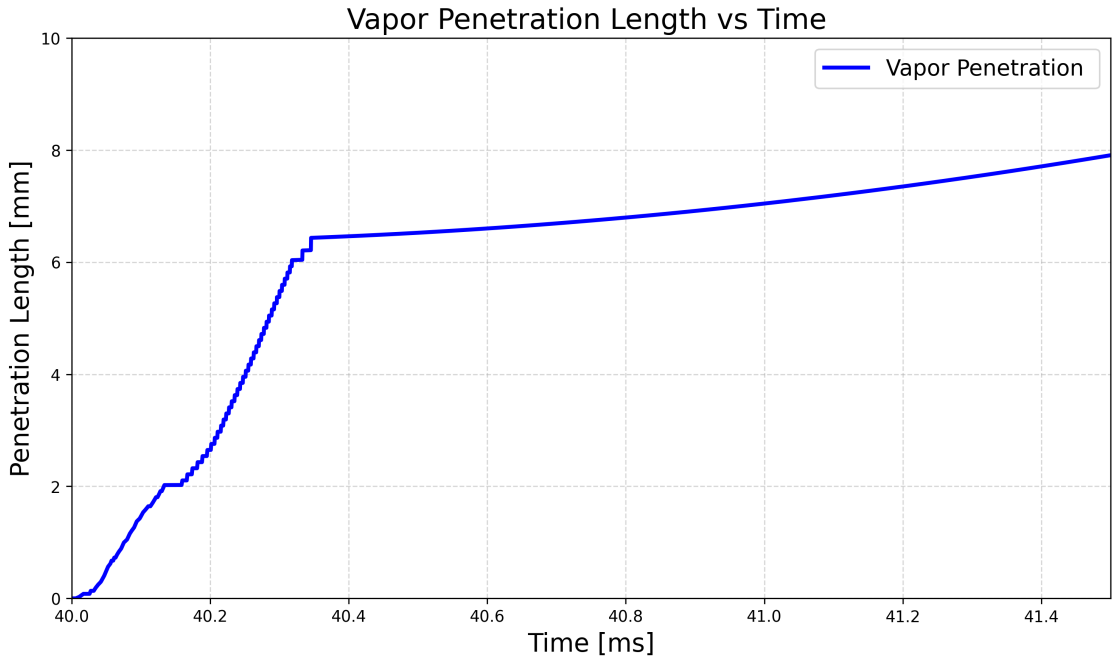

Figure 16: Fuel penetration length inside the cylinder after the start of injection at 40 ms in the compressed state

6 Limitations

- **Delay in liquid penetration**: As shown in fig:7, the initial penetration of the fuel does not show much agreement with the experimental result.
- **Vapor penetration**: Delays in the vapor penetration at the initial stages as illustrated in fig:8 in comparison with experimental data provided by ECN spray A benchmark which might be

due to the slow evaporation of the fuel.

- **Temperature at the exhaust phase of the IC engine simulation with fuel injection**: The temperature at the end of the exhaust show unexpected sudden rise as shown in fig:14d which might be the numerical instabilities.

The results for the complete in-cylinder engine cycle (including intake, compression, fuel injection, expansion and exhaust) have not been directly benchmarked against pre-existing experiments or published simulation data. These results may vary depending on the boundary conditions, mesh quality, model parameters, etc. They serve to show the capability of the setup rather than to validate the quantitative data against real engine measurements.

References

[1] J. C. Beale and R. D. Reitz. Modeling spray atomization with the kelvin-helmholtz/rayleigh-taylor hybrid model. *Atomization and Sprays*, 9(6):623–650, 1999.

[2] G. M. Bianchi and P. Pelloni. Modeling the diesel fuel spray breakup by using a hybrid model. *SAE Technical Paper 1999-01-0226*, 1999.

[3] G. D'Errico and L.-M. Malbec. Numerical investigation of droplet collision models for evaporating sprays. In *ILASS Europe 2012, 24th European Conference on Liquid Atomization and Spray Systems*, 2012. Justification for neglecting collision in evaporating sprays (p. 5).

[4] G. Di Ilio et al. Lagrangian spray modelling in openfoam for high-pressure diesel injection. *International Journal of Engine Research or similar*, 2019.

[5] Engine Combustion Network. ECN Spray A: Baseline n-dodecane spray data. `https://ecn.sandia.gov/diesel-spray-combustion/experimental-configuration/spray-a/`, 2024. Accessed: 2024-12-18.

[6] Engine Combustion Network (ECN). Ecn spray a - liquid penetration (95% mass) - baseline condition a (bkldaal1). Online dataset: `https://ecn.sandia.gov/cvdata/assets/datafiles/liq/bkldaAL1-liq.txt`. Accessed:November, 2025].

[7] G. M. Faeth, L.-P. Hsiang, and P.-K. Wu. Structure and breakup properties of sprays. *International Journal of Multiphase Flow*, 21(Suppl.):99–127, 1995.

[8] Saber Fallah. *Electric and Hybrid Vehicles - Technologies, Modeling and Control: A Mechatronic Approach*. 04 2014.

[9] H. Kahila, A. Wehrfritz, O. Kaario, and V. Vuorinen. Large-eddy simulation of dual-fuel ignition: Diesel pilot effects on ignition delay. *Combustion and Flame*, 203:325–341, 2019. Rosin-Rammler SMD = 6 µm (p. 508).

[10] Sanghoon Lee and Sungwook Park. Characterization of the spray atomization process of a multi-hole gasoline direct injector based on measurements using a phase doppler particle analyser. *Proceedings of the Institution of Mechanical Engineers, Part D: Journal of Automobile Engineering*, 227(7):907–920, 2013.

[11] G. M. Magnotti and C. L. Genzale. Exploration of turbulent atomization mechanisms in diesel sprays using high-speed diffraction-based droplet sizing. *International Journal of Engine Research*, 17:103–117, 2016.

[12] Adrian Pandal, José M. Pastor, Raul Payri, Alan Kastengren, Daniel Duke, Katarzyna Matusik, Jhoan S. Giraldo, Christopher F. Powell, and David P. Schmidt. Computational and experimental investigation of interfacial area in near-field diesel spray simulation. *SAE International Journal of Fuels and Lubricants*, 10(2):423–431, 2017.

[13] L. M. Pickett, C. L. Genzale, G. Bruneaux, L. M. Malbec, L. Hermant, C. Christiansen, and J. Schrader. Comparison of diesel spray combustion in constant volume vessels using shadowgraph and dbi imaging. In *Proceedings of the 23rd Annual Conference on Liquid Atomization and Spray Systems (ILASS)*, 2011.

[14] Lyle M. Pickett, Caroline L. Genzale, Gilles Bruneaux, Caspar Christiansen, Louis-Marie Malbec, Laurent Hermant, and Jesper Schramm. Comparison of diesel spray combustion in different high-temperature, high-pressure facilities. *SAE International Journal of Engines*, 3(2):156–181, 2010.

[15] R. D. Reitz. Modeling atomization processes in high-pressure vaporizing sprays. *Atomisation and Spray Technology*, 3:309–337, 1987.

[16] L. Schiller and A. Naumann. A drag coefficient correlation. *Zeitschrift des Vereins Deutscher Ingenieure*, 77:318–320, 1933.

[17] Schmidt D. P. Nouar I. Rutland C. J. Reitz R. D. Senecal, P. K. Modeling high-speed viscous liquid sheet atomization. *Journal of Multiphase Flow*, 25(6–7):1073–1097, 1999.

[18] D. B. Spalding. *Some Fundamentals of Combustion*. Butterworths Scientific Publications, 1955.

[19] A. Wehrfritz. Large eddy simulation of high-velocity fuel sprays: Studying mesh resolution and breakup modeling effects. Master's thesis, Aalto University, 2013. Table 3 for Rosin-Rammler exponent n=3.